Two-photon optogenetics of dendritic spines and neural circuits

Adam M Packer[1,2,5,6], Darcy S Peterka[1,2,6], Jan J Hirtz[1], Rohit Prakash[3,4], Karl Deisseroth[3,4] & Rafael Yuste[1,2]

We demonstrate a two-photon optogenetic method that generates action potentials in neurons with single-cell precision, using the red-shifted opsin C1V1$_T$. We applied the method to optically map synaptic circuits in mouse neocortical brain slices and to activate small dendritic regions and individual spines. Using a spatial light modulator, we split the laser beam onto several neurons and performed simultaneous optogenetic activation of selected neurons in three dimensions.

Temporally precise control of neuronal firing with single-cell precision is a long-sought goal in neuroscience. Although optogenetics allows optical manipulation of genetically defined populations of neurons[1,2], typical experiments use visible light, which targets all opsin-expressing neurons simultaneously and does not permit spatiotemporal manipulation of neuronal activity at the single-cell level. Two-photon photostimulation offers single-cell resolution[3–6], but it has been used for optogenetics in only a few instances[4–7]. Among the reasons for this are the limitations imposed by current opsins. Although channelrhodopsin-2 (ChR2) has a high two-photon excitation cross-section[4], its single-channel conductance is low, and it displays fast kinetics[8], so the net charge injected per channel is small. This, combined with the small two-photon excitation volume, means that for two-photon activation of a neuron with ChR2, one typically needs either very high opsin expression or relatively complex stimulation strategies[4–7,9].

To practically combine two-photon microscopy with optogenetics, we sought to make it possible to activate single cells expressing moderate levels of opsins with standard (galvanometer-based) scanning microscopes. We used C1V1$_T$, a new red-shifted chimeric opsin formed by combining ChR1 and VChR1 (ref. 1), which has significant two-photon absorption above 1,000 nm and slower channel kinetics[10]. We infected the somatosensory cortex of adult mice with adeno-associated viruses (AAVs) containing the *C1V1$_T$* and *EYFP* genes, under the control of the *CaMKII* promoter, and after 4 weeks we made neocortical slices and performed two-photon imaging on them (**Fig. 1a** and Online Methods). We found large cortical territories with EYFP-labeled neurons, which were assumed to also express C1V1$_T$ (**Fig. 1b**). The area with EYFP-expressing cells extended over 1,200 µm, with strongest expression over the central 750-µm zone, particularly in cortical layers 2, 3 and 5. Using two-photon imaging, we could identify individual neuronal somata and dendritic and axonal processes across all cortical layers (**Fig. 1c**,**d**). We patched fluorescently labeled cells and first activated these neurons with blue light (mercury arc lamp, band-pass 470–490 nm, 20×/0.5–numerical aperture (NA) objective, 0.3 mW mm^{-2} on sample) while measuring currents by voltage clamp. Photostimulated currents exhibited a large range of steady-state one-photon currents even near the highest expression area (754 ± 403 (mean ± s.d.) pA, range 40–1,870 pA, $n = 58$; **Fig. 1e**). We then performed two-photon stimulation (1,064 nm) of targeted cells by raster scanning a small square region of interest (ROI) on the cellular somata. Incrementally increasing the light power on the sample from 1 to 41 mW produced stronger currents, which saturated at hundreds of picoamperes (**Fig. 1f**). For individual neurons, the ratio of photocurrents produced by wide-field one-photon excitation to those produced by two-photon somatic restricted ROI scanning (30 mW) was nearly constant (6.9 ± 2.8 (mean ± s.d.), $n = 23$, $R = 0.76$). Because of this, one-photon photocurrents can predict two-photon responses.

We optimized the two-photon scanning parameters to produce high peak photocurrents (**Fig. 1g** and Online Methods) and chose 2-ms-per-line scanning of a 32 × 32–square–pixel ROI as the optimal scanning profile (which results in a 73.4-ms photostimulation). This protocol reliably generated action potentials (APs) in current-clamp recordings (**Fig. 1h**). The spatial resolution of the two-photon stimulation using this scanning pattern enabled single-cell precision in firing of individual cells (full-width at half maximum (FWHM) = 6.5-µm lateral resolution, 29.5-µm axial resolution; **Supplementary Fig. 1**). Generally, only one AP was generated per raster scan (1.18 ± 0.56 (mean ± s.d.), $n = 795$ photostimulations), although neurons expressing high levels of opsin (as inferred from their high one-photon photocurrents, that is, >1 nA) sometimes produced two or three APs under two-photon stimulation. Latencies from the start of the scan to the peak of the first AP were reproducible across cells (58 ± 12 ms (mean ± s.d.), $n = 16$ cells; **Fig. 1h**) and were shorter with both increased expression and increased light power on the sample ($R = 0.2$ and 0.4; data not shown). The AP jitter, defined as the s.d. of the latency, was 11 ± 7.7 ms (mean ± s.d., $n = 15$ cells). AP latency increased with subsequent stimulations under excitation frequencies of >0.1 Hz

[1]Howard Hughes Medical Institute (HHMI), Columbia University, New York, New York, USA. [2]Department of Biological Sciences, Columbia University, New York, New York, USA. [3]HHMI, Stanford University, Stanford, California, USA. [4]Department of Bioengineering, Stanford University, Stanford, California, USA. [5]Present address: Wolfson Institute for Biomedical Research, University College London, London, UK. [6]These authors contributed equally to this work. Correspondence should be addressed to R.Y. (rafaelyuste@columbia.edu).

RECEIVED 1 OCTOBER; ACCEPTED 19 OCTOBER; PUBLISHED ONLINE 11 NOVEMBER 2012; DOI:10.1038/NMETH.2249

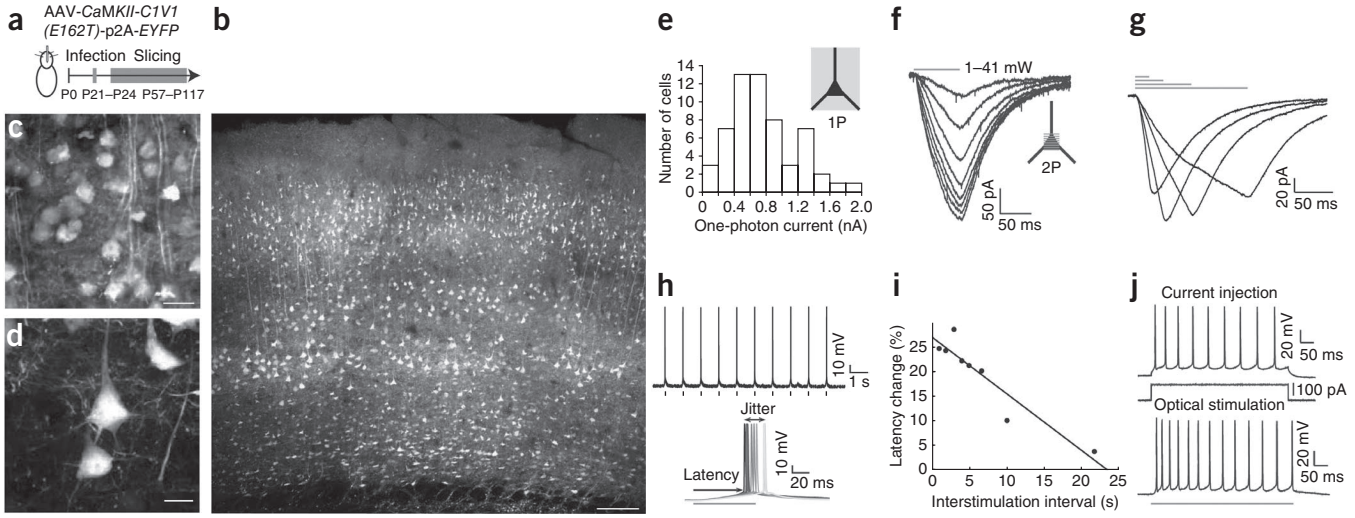

Figure 1 | Two-photon activation of individual neurons with C1V1$_T$ in mouse brain slices. (**a**) Experimental strategy. AAVs encoding the opsin *C1V1$_T$* and *EYFP* genes were injected into the somatosensory cortex of a mouse. Several weeks later, brain slices were made from the infected region. (**b**) Two-photon fluorescence image of a living cortical brain slice expressing EYFP (940-nm excitation, 15 mW on sample, 25×/1.05-NA objective; scale bar, 100 µm). (**c**,**d**) Higher-magnification images from **b** showing C1V1$_T$-expressing cells in upper (**c**) and lower (**d**) layers (scale bars, 20 µm (**c**) and 10 µm (**d**)). (**e**) Distribution of steady-state currents elicited by one-photon (1P) wide-field stimulation, measured with voltage-clamp recordings from C1V1$_T$-expressing cells (mercury arc lamp, band-pass 470–490 nm, 20×/0.5-NA objective, 300 µW mm^{-2}, 150 ms illumination time). Gray box illustrates stimulated area. (**f**) Two-photon (2P) photocurrents measured with voltage clamp in a C1V1$_T$-expressing neuron under different illumination light powers. The raster-scan pattern (inset, gray lines) across a neuronal cell body had 32 lines, 2 ms per line and bidirectional scanning (1,064 nm, 1–41 mW on sample, 20×/0.5-NA objective). (**g**) Two-photon photocurrents induced in C1V1$_T$-expressing neurons under different scan-duration times (gray lines correspond to 0.5, 1, 2 and 4 ms per line; experimental parameters as in **f**). (**h**) Top, current-clamp recordings from C1V1$_T$-expressing neurons during two-photon illumination (stimulated at tick marks; experimental parameters as in **f**). Bottom, overlay of APs generated by two-photon illumination (gray bar). (**i**) Quantification of AP latency changes from experiments as in **h** with different stimulation intervals. (**j**) Spiking patterns resulting from either a current injection at four times rheobase (top) or from an optical stimulation produced by continuously raster scanning the cell body for the same time duration (bottom; other experimental parameters as in **f**).

(R^2 = 0.8; **Fig. 1i**). Prolonged photostimulation produced APs at frequencies exceeding those of four times rheobase (**Fig. 1j**).

We then used two-photon illumination of C1V1$_T$ to stimulate single dendrites and spines. We selected cells exhibiting high EYFP expression and raster-scanned individual dendritic processes, using the same patterns used to successfully generate photocurrents in somata (23 ± 11 pA (mean ± s.d.), range 7–49 pA, n = 21 dendrites and 8 neurons; **Fig. 2a**). Dendrites located further from the soma yielded lower currents (R = 0.45; **Supplementary Fig. 2**). We also targeted spines and dendrites with point excitation, which elicited smaller currents (**Fig. 2b** and **Supplementary Table 1**). We did not elicit photocurrents when we moved the laser a few micrometers away from the targeted spines or dendrites (**Supplementary Fig. 3**). Mean peak currents for point stimulation were similar for spines (7.1 ± 1.58 pA (± s.d.), n = 8) and dendrites (6.0 ± 1.14 pA, n = 4; Mann-Whitney, P = 0.33). Mean 10%–90% rise time was also similar for spines (15.5 ± 4.16 ms (± s.d.), n = 8) and dendrites (15.6 ± 5.73, n = 5; Mann-Whitney, P > 0.99). Latencies for point photostimulation of spines and dendrites were always less than 3 ms (**Supplementary Table 1**), and the decay kinetics of both were also similar, >60 ms (data not shown). Spines and dendrites of weakly or non-expressing cells (n = 4), showed no response under identical photostimulation conditions (n = 3 spines and 3 dendrites; data not shown).

A useful application of two-photon photostimulation is optical mapping of synaptic circuits[3], so we explored whether this was possible with C1V1$_T$. We patched pyramidal neurons (n = 36) and monitored time-locked excitatory postsynaptic currents (EPSCs) while raster scanning cell bodies of neighboring EYFP-fluorescent cells to identify presynaptically connected neurons (**Supplementary Fig. 4**). We found many instances in which photostimulating a neuron generated time-locked EPSCs in the patched cell (**Fig. 2c**). Increases in laser power often revealed time-locked EPSCs from neurons that originally did not generate them, presumably by inducing the presynaptic neuron to spike (**Supplementary Fig. 5**). We tested 169 possible presynaptic neurons, of which 8 were identified as connected to the postsynaptic cell on the basis of the kinetics of the time-locked EPSCs generated. In these cases, the amplitude and rise-time kinetics of optically evoked EPSCs matched those of monosynaptic EPSCs observed between pairs of connected pyramidal neurons, targeted randomly (**Supplementary Fig. 6a**; EPSCs amplitudes: 17.5 ± 12.8 pA (mean ± s.d.), n = 16 pairs for paired-recordings versus 15.6 ± 12.7 pA, n = 8 for optically stimulated; P = 0.72, t-test. EPSC rise time: 2.17 ± 0.69 ms (mean ± s.d.), n = 16 for paired recordings versus 2.3 ± 1.1 ms, n = 8 for optically stimulated; P = 0.54, Mann-Whitney). Currents generated by direct stimulation of the postsynaptic cell's dendritic arbor were easy to distinguish from EPSCs because the rise times and latencies did not overlap (**Supplementary Fig. 6**). These differences—and the high spatial resolution of the system (**Supplementary Fig. 1**)—implied that we were accurately detecting presynaptic neurons. We confirmed this by patching putative presynaptic neurons (**Fig. 2d**) as well as putatively unconnected ones. Every electrically tested pair matched the optical prediction (n = 5: two connected, three unconnected).

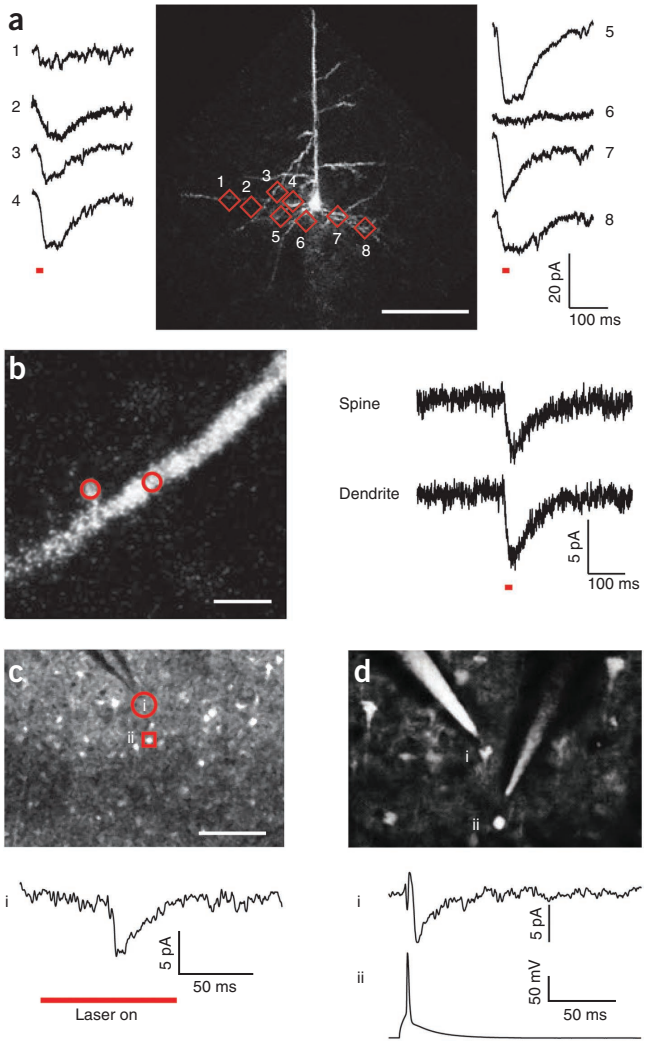

Figure 2 | Two-photon stimulation of individual dendrites and spines and optical mapping of connected neurons. (**a**) Photostimulation of cellular processes. Center, two-photon fluorescence image of a C1V1$_T$-expressing neuron (940 nm, 15 mW on sample, 20×/0.5-NA objective). The cell was patched, and different regions of its dendritic and axonal arbor were scanned with a two-photon laser (numbered red boxes) while somatic currents were simultaneously measured (left and right traces; red bars are photostimulations). Photostimulation parameters: 1,064 nm, 30 mW on sample, 20×/0.5 NA, 32 × 32–pixel ROI and 2 ms per line. Scale bar, 100 µm. (**b**) Left, two photon image of a similar experiment, but stimulating a spine head and dendritic shaft (red circles) from a highly expressing neuron (scale bar, 3 µm). Imaging parameters as in **a**. Right, whole-cell measurements of somatic currents during point stimulation (gray bar; averages of 12). Photostimulation parameters: 1,064 nm, 30 mW on sample, 20×/0.5 NA and 20-ms point stimulation. (**c**) Mapping presynaptic connections. Top, two-photon fluorescence image of a field of neurons expressing C1V1$_T$ (940 nm, 15 mW on sample, 20×/0.5-NA objective). Neuron **i** (red circle) was patched, and surrounding fluorescent neurons were photostimulated while EPSCs in neuron **i** were monitored. Scale bar, 100 µm. Photostimulation parameters: 1,064 nm, 30 mW on sample, 20×/0.5-NA, 32 × 32 ROI and 2 ms per line. Bottom, EPSCs in neuron **i** during photostimulation of neuron **ii** (average of 12). (**d**) Same experiment as in **c**, after dual whole-cell recording was established from neuron **ii** (red square). Top, two-photon fluorescence image from both neurons with identical imaging parameters as in **c** (scale bar, 50 µm). Bottom, simultaneous voltage-clamp recording from neuron **i** and current-clamp recordings from neuron **ii**.

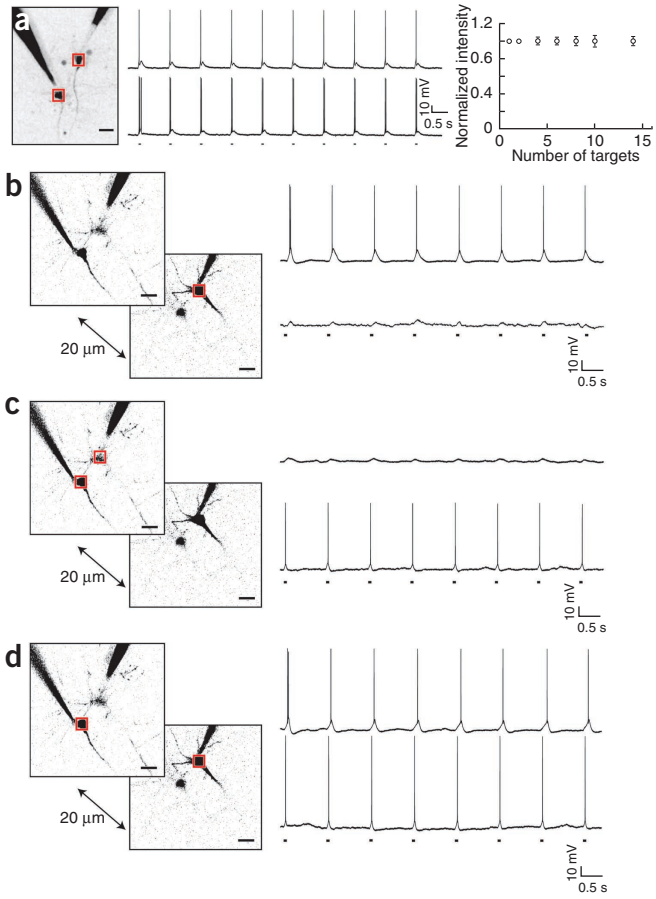

Figure 3 | Two-photon 3D stimulation of two individual neurons with SLMs. (**a**) Left, two-photon fluorescence image of two C1V1$_T$-expressing neurons located in the same focal plane, which were patched. Imaging parameters: 940 nm, 15 mW on sample, 20×/0.5-NA objective. Image lookup table is inverted for clarity. An SLM phase mask was calculated to generate one photostimulation laser spot for each cell, and both laser spots were then raster scanned simultaneously across the cell bodies (boxes). Photostimulation parameters: 1,064 nm, 30 mW per target, 32 × 32 ROI, 2 ms per line. Center, whole-cell current-clamp recordings from both cells during two-photon SLM photostimulation (black marks). Right, light intensity generated by different numbers of SLM targets in similar experiments (**Supplementary Fig. 9**; 3–15 measurements per target; error bars, s.d.). (**b**) Depth selectivity of SLM photostimulation. Left, two-photon fluorescence image of two C1V1$_T$-expressing neurons located 20 µm apart in depth, which were patched. A single-beam SLM stimulation spot was scanned (box). Imaging parameters as in **a**. Right, whole-cell current-clamp recordings from both neurons during photostimulation of one of them (black marks; black box in left) with the SLM spot. Photostimulation parameters: 1,064 nm, 30 mW on one target, 32 × 32 ROI, 2 ms per line. (**c**) Experiment as in **b** but using a 2D two-beam SLM pattern. Left, two-photon fluorescence image of two neurons. Imaging as in **a**. A new SLM pattern was scanned in the superficial focal plane in the position corresponding to the two cells (boxes). Right, simultaneous dual whole-cell recordings during photostimulation (black marks). Photostimulation parameters: 1,064 nm, 30 mW per target, 32 × 32 ROI, 2 ms per line. (**d**) Experiment as in **c** but with a 3D SLM pattern, which directed two laser beam spots onto both cells simultaneously. Left, two-photon fluorescence image of both neurons illustrating the simultaneous, multifocal SLM stimulation (boxes). Imaging parameters as in **c**. Right, simultaneous dual whole-cell recordings during photostimulation (black marks). Photostimulation SLM parameters as in **c**. Scale bars, 20 µm.

In one connected pair, hyperpolarizing the presynaptic cell prevented optical activation and the appearance of time-locked EPSCs, confirming that the patched connected neuron was the unique source of the observed current (**Supplementary Fig. 7**). Finally, we photostimulated two putative presynaptic neurons, with brief (12-ms) intervals between stimulations. This generated trains of postsynaptic EPSCs (inter-EPSC intervals ranged 81–168 ms), with a paired-pulse ratio of 0.68 ± 0.03 (mean ± s.d., $n = 2$ neurons; **Supplementary Fig. 8**). This synaptic depression is often found in neocortical excitatory connections[3], so it may be possible to optically map short-term synaptic plasticity using this methodology.

Last, we explored the use of C1V1$_T$ for two-photon spatial light modulator (SLM)-based microscopy, a holographic method that enables optical targeting of groups of neurons or spines located in arbitrary three-dimensional (3D) positions[11,12]. We first projected two laser beams of equal power onto two C1V1$_T$-expressing cells and confirmed with paired recordings that APs were generated simultaneously in both cells (**Fig. 3a**; $n = 6$ pairs). Increasing the number of optically targeted neurons to 15 could still reliably trigger APs in the monitored cells ($n = 3$), and we confirmed that similar light powers were delivered to each of the 15 positions (**Fig. 3a**, **Supplementary Fig. 9** and Online Methods). We then used SLM targeting to perform 3D photostimulation of neurons. We first patched a C1V1$_T$-expressing neuron, moved the objective to a different focal plane and photostimulated the cell with an SLM pattern (single or multiple spots) calculated to focus at the cell's plane. With this approach, APs were reliably generated in neurons positioned at axial planes different than the objective plane ($n = 7$ neurons; **Fig. 3b**), confirming that focusing the laser beam with the SLM did not degrade its resolution. We then performed dual whole-cell recordings from neurons located at two different depths ($\Delta z \approx 20$ µm) and split the laser beam into two independent beamlets of equal power. When the beamlets were targeted to a single focal plane coinciding with one of the two neurons, only that neuron generated an AP (**Fig. 3c**). But when we targeted the beamlets to both planes, we were able to elicit APs in both neurons simultaneously (**Fig. 3d**). This shows that, by altering the SLM pattern and without refocusing the objective, we could independently photostimulate two cells located in different planes without cross-stimulation ($n = 2$ pairs).

Using C1V1$_T$ and standard two-photon laser scanning, we demonstrate an efficient combination of optogenetics and two-photon microscopy, enabling precise activation of individual neurons and dendritic spines. The method also allows optogenetic-based mapping of presynaptic neurons and may permit studies of synaptic weights and dynamics. Finally, by generating multiple laser beams with SLMs, several neurons can be selectively or simultaneously activated in three dimensions—an approach that could enable the optical dissection of the function of microcircuits with single-cell precision.

METHODS

Methods and any associated references are available in the online version of the paper.

Note: Supplementary information is available in the online version of the paper.

ACKNOWLEDGMENTS

We thank M. Agetsuma and Y. Shin for assistance with viral injections and surgeries, and other members of the laboratory for help and comments. R.Y., A.M.P., J.J.H. and D.S.P. are supported by the HHMI, Kavli Institute for Brain Science, National Eye Institute, Keck Foundation, Deutsche Forschungsgemeinschaft (DFG grant HI 1728/1-1 to J.J.H.) and Department of Defense Multidisciplinary University Research Initiative Program. R.P. is supported by the US National Institute of Mental Health. K.D. is supported by the HHMI, US National Institutes of Health, California Institute for Regenerative Medicine, Gatsby Foundation and Defense Advanced Research Projects Agency Reorganization and Plasticity to Accelerate Injury Recovery Program.

AUTHOR CONTRIBUTIONS

A.M.P., D.S.P. and R.Y. designed and built the microscope software and hardware. A.M.P., D.S.P. and J.J.H. performed experiments, data analysis and quantification. R.P. and K.D. provided viral constructs, technical assistance, advice and opsin characterization. A.M.P., D.S.P., J.J.H. and R.Y. contributed to the writing of the manuscript.

COMPETING FINANCIAL INTERESTS

The authors declare no competing financial interests.

Published online at http://www.nature.com/doifinder/10.1038/nmeth.2249.
Reprints and permissions information is available online at http://www.nature.com/reprints/index.html.

1. Yizhar, O., Fenno, L.E., Davidson, T.J., Mogri, M. & Deisseroth, K. *Neuron* **71**, 9–34 (2011).
2. Kätzel, D., Zemelman, B.V., Buetfering, C., Wölfel, M. & Miesenbock, G. *Nat. Neurosci.* **14**, 100–107 (2011).
3. Nikolenko, V., Poskanzer, K.E. & Yuste, R. *Nat. Methods* **4**, 943–950 (2007).
4. Rickgauer, J.P. & Tank, D.W. *Proc. Natl. Acad. Sci. USA* **106**, 15025–15030 (2009).
5. Andrasfalvy, B.K., Zemelman, B.V., Tang, J. & Vaziri, A. *Proc. Natl. Acad. Sci. USA* **107**, 11981–11986 (2010).
6. Papagiakoumou, E. *et al. Nat. Methods* **7**, 848–854 (2010).
7. Oron, D., Papagiakoumou, E., Anselmi, F. & Emiliani, V. *Prog. Brain Res.* **196**, 119–143 (2012).
8. Feldbauer, K. *et al. Proc. Natl. Acad. Sci. USA* **106**, 12317–12322 (2009).
9. Zhu, P. *et al. Front. Neural Circuits* **3**, 21 (2009).
10. Mattis, J. *et al. Nat. Methods* **9**, 159–172 (2012).
11. Nikolenko, V. *et al. Front. Neural Circuits* **2**, 5 (2008).
12. Lutz, C. *et al. Nat. Methods* **5**, 821–827 (2008).

ONLINE METHODS

Viral infection, slice preparation and electrophysiology. Animal handling and experimentation were done according to the US National Institutes of Health and Columbia Institutional Animal Care and Use Committee guidelines. Animals of both sexes were used and were housed and maintained in a temperature-controlled environment on a 12-h light-dark cycle, with *ad libitum* food and water, in a Columbia University Animal Facility. We injected C57BL/6 mice aged postnatal day (P) 21 to P24 with 750–850 nL of AAV-*CaMKII-C1V1$_T$(E162T)*-p2A-*EYFP* at a rate of 130 nL/min at a depth of 400 µm from the pial surface of the somatosensory cortex using a UMP3 microsyringe pump (World Precision Instruments). After a wait of at least 4 weeks, acute coronal slices 350 µm thick were prepared from P57–P210 mice using a Leica VT1200S vibratome after cardiac perfusion with ice-cold sucrose solution containing the following (in mM): 27 $NaHCO_3$, 1.5 NaH_2O_4, 222 sucrose, 2.5 KCl, 3 $MgSO_4$ and 1 $CaCl_2$. Slices were incubated at 36 °C for 30 min in ACSF containing (in mM): 126 NaCl, 26 $NaHCO_3$, 1.1 NaH_2O_4, 10 glucose, 3 KCl, 3 $MgSO_4$ and 1 $CaCl_2$. During recordings, ACSF was similar except for (in mM): 2 $MgSO_4$ and 2 $CaCl_2$. Sucrose and ACSF solutions were saturated with 95% O_2 and 5% CO_2. Whole-cell recordings were made through 5- to 6-MΩ glass pipettes using Axon Multiclamp 700B amplifiers (Molecular Devices), digitized at 10 kHz with National Instruments 6259 multichannel cards and recorded using custom software written using LabView (National Instruments). Intracellular solution, pH 7.2, contained (in mM): 135 potassium methylsulfate, 8 NaCl, 10 HEPES, 2 Mg-ATP, 0.3 sodium-GTP, 7 phosphocreatine, 0.02 Alexa Fluor 594 and 10.7 biocytin.

Imaging and photostimulation. Experiments were performed with a custom-made two-photon dual-laser dual-scanning microscope based on a modified Olympus BX50WI microscope with 40×/0.8-NA or 20×/0.5-NA water-immersion objectives (Olympus). Initial photostimulation characterization and mapping experiments were performed using a Ti:sapphire laser as the light source (Coherent Chameleon Ultra II, 140-fs pulses, 80-MHz repetition rate). These experiments using the Ti:sapphire laser were performed at 1,040 nm. Scanning was performed using one of the set of galvanometer mirrors controlled using Fluoview software (Olympus). This scanning system had a low fill fraction (the amount of time spent scanning the marked ROI versus the total scan time), and though successful in triggering APs, it was relatively inefficient, with low peak photocurrents and large jitter and latency.

All other experiments were performed with a second set of scanners on our two-photon laser-scanning and SLM microscope[11]. This beam path used a high-power, fixed-wavelength ultrafast laser (5 W, 1,064 nm, 300-fs pulses at 80 MHz). Galvanometer mirrors (Cambridge Technology) and a reflective HD SLM (Holoeye 1080 HEO) were installed, with the mirrors controlled by ScanImage (Janelia Farm) and the phase mask sent to the SLM via software from Holoeye. Care was taken to ensure raster scans had a high fill fraction to minimize stimulation outside the selected ROI. Optimal raster scans (2 ms per line, **Fig. 2c**) were performed bidirectionally over neuronal cell bodies (32 × 32 pixels, 51.2-µs dwell time per pixel).

Two-photon activation of C1V1$_T$- expressing neurons. To optimize AP generation, we explored the power dependency of the two-photon photocurrents. We obtained significant currents with as little as 1 mW of 1,064-nm light on sample (20×/0.5-NA objective), whereas currents saturated above ~30 mW at a level dependent on the amount of opsin expression. We also optimized the temporal pattern of the photoactivation. For short duration illuminations, the off-time of C1V1$_T$ is ~60 ms (ref. 10), but this may depend on illumination time and intensity. In our experiments, using more extended illuminations (150 ms), we measured an effective off-time of up to 80 ms and chose this as our upper bound for effective scan times. Because the diameter of a typical neuronal soma is ~15–20 µm and the effective PSF produced with the 0.5-NA objective at nonsaturating powers is ~1 µm, we chose to scan the cell ROI with 32 lines, ensuring the complete overlapped coverage of the entire cell. At typical excitation powers (30 mW), values of 0.5 ms per line (17 ms per scan) or shorter were too fast to reach the maximum possible current, perhaps because of insufficient integrated photon fluxes for complete activation of all opsins in the selected volume. Meanwhile, values 4 ms per line or longer (>130 ms per scan) were too slow because, as expected, opsins stimulated in the initial part of the scan were closed before the end of the scan (**Fig. 1g**). Intermediate scan rates of 1–2 ms per line produced higher, nearly identical photocurrents. Given that the ratio of one-photon to two-photon photocurrents is 6:1, and the rheobase of a typical pyramidal neuron is around 100 pA (ref. 13), the expected average one-photon photostimulation current required for successful two-photon activation would be approximately 600 pA. Using the photocurrent histogram (**Fig. 1e**), we estimate that our two-photon stimulation protocol should fire almost 50% of the excitatory neurons at the injection site. This is likely a lower estimate, as many cells with one-photon currents less than 600 pA were two-photon addressable (**Supplementary Fig. 10a**). In layers 2, 3 and 5, where we found high C1V1$_T$ expression, this would imply that, for a single injection, ~10,000 neurons are capable of firing following two-photon photoactivation (48% of all neurons in a sphere 750 µm in diameter, assuming a density of 92,000 neurons per mm (ref. 14)). The mean time of expression of animals in our experiments was 8 ± 2 weeks, but we found no strong correlations of photocurrents with time over that window (**Supplementary Fig. 10b**). Nevertheless, it is possible that with substantially longer expression times, there could be an even a larger pool of two-photon addressable cells. However, we did not find this in the oldest acute slices (>30 weeks post-injection), which showed a reduced number of EYFP-expressing cells and generally reduced viability, perhaps simply because of the age of the animals. Regardless, with judicious choices of photostimulation parameters, single APs were reliably generated in a large fraction of C1V1$_T$-expressing neurons with precise timing using two-photon excitation and simple raster-scanning illumination patterns.

We noticed that trains of photostimulation altered the latencies of the generated APs. The difference between the latency of the first and last AP during a sequence of stimulations (normalized to the latency of the last AP) was 25 ± 1% during an interstimulus interval (ISI) of 1 s but dropped to 4 ± 8% with an ISI of 22 s (**Fig. 1i**). Most neurons appeared to recover their original latencies given sufficient time, indicating that there is a small, subtle

photoinduced process that alters the excitability of the cell and that recovers on the time scale of seconds. We also noticed that although some cells could seemingly be stimulated indefinitely, a small subset of cells became increasingly resistant to optical stimulation, even with increased illumination intensities and longer ISI, despite readily firing action potentials with current injections.

Detection of connections after photostimulation. To accurately predict putative presynaptic neurons, we needed definitive criteria to distinguish monosynaptic EPSCs from currents generated by directly stimulating the dendrites of the postsynaptic neuron. The rise time for direct stimulations was 35.8 ± 19.4 ms (n = 21), more than ten times the rise times for EPSCs and statistically distinct from them (P < 0.0001, unpaired t-test). However, the quickest way to distinguish these responses was by the latency of the response from photostimulation onset: all direct photostimulations started within 3 ms of laser onset, whereas the optically evoked EPSC latency was 54.1 ± 18.6 ms (n = 8, range 29–84 ms). The smallest optically evoked EPSC latency was ten times larger than the largest direct stimulation of the postsynaptic cell's arbor, so the statistical difference between these distributions is very strong (P < 0.0001, unpaired two-tailed t-test). Although we occasionally observed combined events in which a connected presynaptic neuron and a portion of the postsynaptic neuron's arbor were photostimulated simultaneously (**Supplementary Fig. 5d**), the EPSC trace was easy to identify because of the time-locked nature with which it occurs relative to laser onset and the very different kinetics from that of direct stimulation.

The average probability of connection found, 5%, is lower than in younger animals[13], although our data are the first we are aware of to probe excitatory connectivity at a large scale in older animals. This low connectivity also indicates that two-photon photostimulation did not cause widespread axonal activation.

Spatial light modulator microscopy. In this study, we applied spatial light modulators (SLMs) to generate arbitrary spatio-temporal patterns of light[6,11,12,15–17]. In our setup, the laser beam was expanded to fill the reflective SLM surface, which displayed phase masks that modulated the wave front of the incoming laser beam such that multiple beamlets were generated in the far field (such as on the sample). Each individual beamlet targeted different neurons in the nominal focal plane of the microscope. These targeted multibeam patterns were coupled into the microscope through galvanometer mirrors that enabled raster scanning of the individual laser beam spots across multiple ROIs. 2D phase masks for the SLM were generated by either software provided by Holoeye software or custom code running in Matlab[3], whereas the 3D patterns were generated exclusively with custom code in Matlab using either a simple prism-lens approach[18] or a paralleled multiplane optimization algorithm[19].

For individual neurons, the lateral resolution, defined by the full-width at half maximum (FWHM) of the spiking probability, was 6.9 µm, and the axial resolution was 29.5 µm and was identical to that of normal, single-beam targeting with the same objective, confirming that beam splitting with the SLM does not significantly degrade the PSF (**Supplementary Fig. 1**)[11]. The high lateral resolution ensures that, as soon as the cell body was partially outside of the raster-scanned ROI, the spiking probability drops sharply, and it implies that it is critical to illuminate a substantial portion of the somatic membrane to generate APs. As expected, the induced subthreshold photocurrents decayed more slowly (**Supplementary Fig. 1a**, gray dashed curve). The lower axial resolution was expected, and it corresponds to the axial extent of the neuron's cell body convolved with the two-photon PSF generated by the 20×/0.5-NA objective. Thus, the SLM microscope was reliable and accurate in generating APs in two neurons simultaneously.

To ensure that the optically induced spiking of the single patched neuron would be considered representative of all of the other neurons, we verified that the illumination intensity of the beamlets was identical in subsequent measurements: immediately following the multiplexed optical-activation experiments, the sample was changed to a uniformly fluorescent, liquid-filled microcapillary (50 µM rhodamine 6) and illuminated with the same multiplexed beamlet producing phase masks on the SLM. We measured the two-photon–produced fluorescence generated by each individual beamlet and observed that there were no significant variations in the intensity of the multiple beamlets (**Fig. 3a**, right). On the basis of these measurements, we expected that every one of the additional neurons illuminated by the SLM patterns would fire APs as the recorded cell did. We similarly monitored for 'stray' excitation areas, or reductions in the lateral confinement or focusing of the individual multispot targets, and detected no significant effects (**Supplementary Fig. 9c–e**). Considering our power budget and the overall efficiency of our SLM microscope system (we can deliver almost 1 W on the sample across multiple targets), we anticipate targeting capability for up to 40 pyramidal cells simultaneously within a 500-µm FOV.

Because SLMs are essentially universal optics, they can also act as a focusing lens, and the focal position of the laser beam in the sample can be moved independently, in software and without any mechanical devices, relative to the objective's focal plane[11]. The volume that can be addressed by the SLM in our microscope for a given sample and galvanometer mirror position is determined by the SLM pixel pitch and overall effective magnification; this volume was a cylinder 520 µm in diameter and 400 µm tall (20×/0.5-NA objective). Although there were variations in the PSF through this focused volume, because of changes in the effective NA of the objective due to the additional lens function, and to chromatic effects from the diffractive optic (SLM), the effective cell-targeting resolution did not change significantly. Although one would expect more substantial degradations with a higher NA, for the purposes of activating somata with two-photon photostimulation, lower-NA objectives are actually beneficial[4]. An additional complication of using the SLM as a focusing device is that the nominal magnification factor of the microscope changes as the focal plane is adjusted because the beam is no longer strictly collimated between the tube lens and the objective focal plane. Fortunately, this change is linear and could be easily calibrated (14% increase per focal plane displacement of 100 µm; **Supplementary Fig. 9a**). Similar effects were recently seen in a novel microscope using an electrotunable lens for fast axial focusing[20]. This change in magnification would begin to affect the lateral resolution of our raster-scanned stimulation protocol if cells were simultaneously targeted and scanned across vastly different axial planes. For these particular instances, a more complex stimulation strategy may be required.

doi:10.1038/nmeth.2249

In our 'out of focal plane' photoactivation experiments, there was no apparent change in the axial resolution of AP generation in the subset of addressable SLM volume that was examined, which was ±120 µm around the nominal focal plane of the objective (FWHM of AP probability versus axial distance = 28 ± 5 µm, $n = 9$ focal planes; steps of 15 µm, in addition to zero lens phase corresponding to objective focal plane). An identical result was seen in an experiment monitoring the peak photocurrents generated by optical stimulation of a cell at different focal planes (**Supplementary Fig. 9b**).

13. Lefort, S., Tomm, C., Floyd Sarria, J.-C. & Petersen, C.C.H. *Neuron* **61**, 301–316 (2009).
14. Schüz, A. & Palm, G. *J. Comp. Neurol.* **286**, 442–455 (1989).
15. Nikolenko, V., Peterka, D.S. & Yuste, R. *J. Neural Eng.* **7**, 045001 (2010).
16. Yang, S. *et al. J. Neural Eng.* **8**, 046002 (2011).
17. Maurer, C., Khan, S., Fassl, S., Bernet, S. & Ritsch-Marte, M. *Opt. Express* **18**, 3023–3034 (2010).
18. Daria, V.R., Stricker, C., Bowman, R., Redman, S. & Bachor, H.-A. *Appl. Phys. Lett.* **95**, 093701 (2009).
19. Piestun, R. & Shamir, J. *Proc. IEEE* **90**, 222–224 (2002).
20. Grewe, B.F., Voigt, F.F., van't Hoff, M. & Helmchen, F. *Biomed. Opt. Express* **2**, 2035–2046 (2011).